Available online at www.sciencedirect.com
ScienceDirect
Journal of Power Sources 179 (2008) 785–792
JOURNAL OF POWER SOURCES
www.elsevier.com/locate/jpowsour

Short communication

Calendar life study of Li-ion pouch cells Part 2: Simulation

Qi Zhang, Ralph E. White *

Center for Electrochemical Engineering, Department of Chemical Engineering, University of South Carolina, Swearingen Engineering Center, 301 Main Street, Columbia, SC 29208, USA

Received 23 October 2007; received in revised form 6 December 2007; accepted 7 December 2007
Available online 22 January 2008

Abstract

The low rate (C/33) discharge data obtained from a calendar life study were numerically analyzed with a single particle model. The simulation showed that the stoichiometric window for the cathode shrank with capacity fade. The change of the stoichiometric window for the anode was more complicated. The aged anode became less charged when the capacity fade was caused mostly by the loss of cyclable lithium ions. The anode would be charged to a higher stoichiometric number (or state of charge, SOC) when the capacity fade became controlled by the loss of active material in the anode.

Keywords: Calendar life; Stoichiometric window; Active material loss

1. Introduction

Lithium ion batteries have been widely used in consumer electronics and they are being actively researched for automobile, satellite and many other applications. A few papers [1–3] are found in the literature to study numerically the capacity fade phenomenon during the life testing of lithium ion batteries. Liaw et al. [1] used a relatively simple equivalent circuit model (ECM) to study the capacity fade in a calendar life study. They were able to achieve high fidelity simulation results with a consistent set of parameters. Yet the parameters of the ECM model mostly do not correspond directly to the physical parameters of the lithium ion batteries, which is a major drawback of the method. Stamps et al. [2] studied the capacity fade of a lithium ion cell over 1600 cycles using a hybrid estimation algorithm combining elements of both batch estimation and online moving horizon estimation. The methodology offers the ability to monitor the long-term conditions of the battery while minimizing the noise attributable to the cycle-to-cycle variation. The battery model was nevertheless oversimplified in their work. Ramadass et al. [3] used a semi-empirical model to study the capacity fade of Sony 18650 cells. The empirical correlations for the initial state of charge (SOC) and the surface film resistance of the negative electrode were established by simulating the experiment data at selected cycles. These numerical studies were able to provide useful information about the capacity fade of the cells in addition to the experiment studies.

Recently we reported [4] our experiment results on a calendar life study. The loss of active materials in the electrodes and the loss of cyclable lithium ions were found to be the major capacity fade mechanisms responsible for the cell capacity fade at low C/33 rate. However, the experiment provided little information about whether or not the two mechanisms played an equally important role throughout cell capacity fade. In the work reported here, the experimental data were numerically analyzed to answer the question. Furthermore, the change of stoichiometric windows of the individual electrodes with capacity fade is discussed in details based on our simulation results.

2. Experimental

The experiment details of the calendar life study were revealed in a previous paper [4]. The test procedures were summarized in Fig. 1. The procedures included rate capability tests,

* Corresponding author. Tel.: +1 11 803 777 3270; fax: +1 11 803 777 0973.
E-mail address: white@engr.sc.edu (R.E. White).

0378-7753/$ – see front matter © 2007 Elsevier B.V. All rights reserved.
doi:10.1016/j.jpowsour.2007.12.022

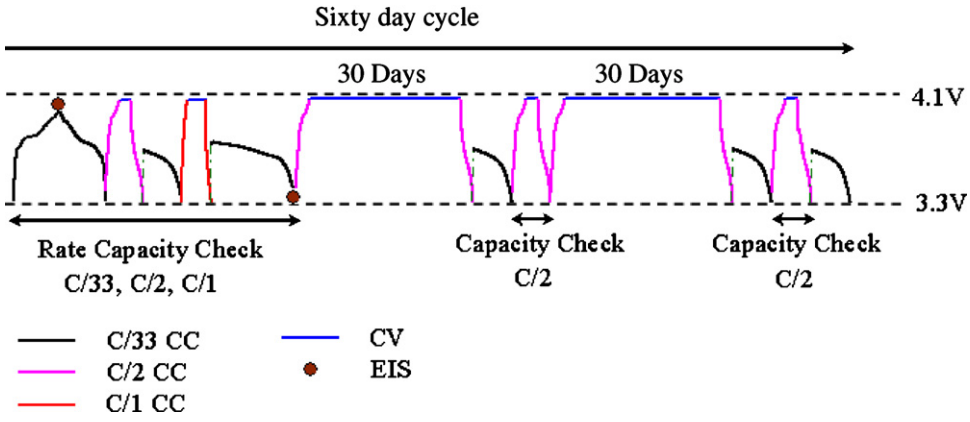

Fig. 1. Schematic diagram of the test procedures for the calendar life study ($C = 1.828$ A). The cells were float charged during storage.

Nomenclature

A	electro-active surface area (cm^2)
c_e	Li^+ concentration in the electrolyte ($mol\,cm^{-3}$)
c_{max}	maximum Li^+ concentration in the particles ($mol\,cm^{-3}$)
c_s	Li^+ concentration in the solid particles ($mol\,cm^{-3}$)
$\bar{c}_s$	volume averaged Li^+ concentration inside spherical particles ($mol\,cm^{-3}$)
c_{se}	Li^+ concentration at the surface of the solid particles ($mol\,cm^{-3}$)
D_s	solid phase Li^+ diffusion coefficient in the particles ($cm^2\,s^{-1}$)
I_{app}	applied current (A)
j_{int}	intercalation current density ($A\,cm^{-2}$)
k	kinetic rate constant $(A\,cm^{-2})/(mol\,cm^{-3})^{1.5}$
n	number of terms in Eq. (5)
R_s	radius of the spherical particles (cm)
U	open circuit potential of the electrode (V)
V	volume of the electrode (cm^3)
$x_{0,i}$	the stoichiometric number of the electrode at charged state
x_i	the stoichiometric number of the electrode at discharged state

Greek letters

ε_s	volume fraction of the active material in the electrode
λ_m	positive eigen-value determined from $\lambda_m = \tan(\lambda_m)$.
Φ	electrode potential (V)

storage at float charge condition (4.1 V) and capacity checks. The experiments were conducted at five temperatures: 5, 15, 25, 35 and 45 °C. The capacity fade measured at the C/33 rate is presented in Fig. 2. The capacity fade at 5 and 15 °C is linear with time, while the nonlinear capacity fade at 25, 35 and 45 °C might also be viewed as two linear capacity fade regimes in sequence.

Our half-cell study [4] showed that the used electrodes harvested from the aged cells had reduced capacities (discharged at very low rate) as compared to fresh electrodes, indicating a loss of active materials in the electrodes with cell capacity fade. Our conclusion [4] is that the loss of active materials in the electrodes and the loss of cyclable lithium ions are the two major capacity fade mechanisms responsible for the cell capacity fade at low C/33 rate.

Nevertheless, the experiment does not supplied answers to the question that whether or not the two mechanisms played an equally important role throughout cell capacity fade, such as the nonlinear capacity fade exhibited at high temperatures. Actually it is quite difficult to answer the question experimentally, because a large sample size of pouch cells and regular destructive analysis are required for that purpose. That is, we need to open a few pouch cells (thus useless for further aging test) regularly during the aging study in order to experimentally measure the severeness of active material loss in individual electrodes.

In this work, an alternative numerical approach was applied to investigate the roles of the two capacity fade mechanisms

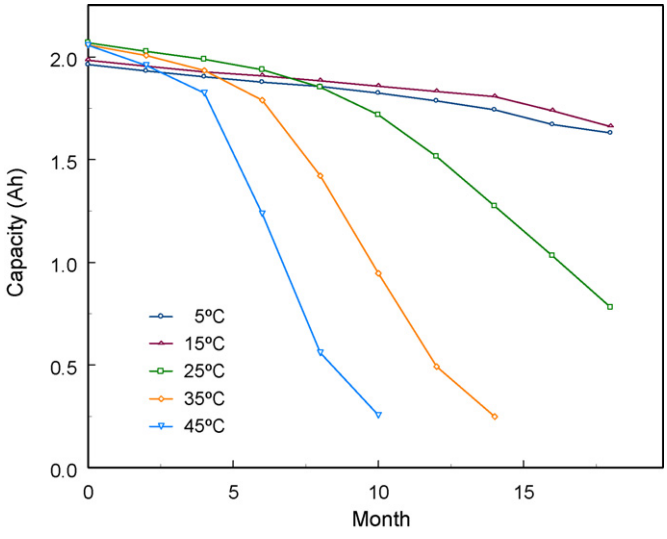

Fig. 2. The capacity fade of the cells in the calendar life study.

at different temperatures. In the following section, a so-called single particle model [5,6] was introduced, and then used to analyze the low rate (C/33) discharge data. The results from our simulation were discussed in details in Section 4.

3. Model

The single particle model [5,6] uses the assumption that the behavior of the porous electrodes can be represented by spherical particles of the active materials in the electrodes. The concentration and potential distributions in the solution phase are assumed to be negligible, which is a reasonable assumption under low rate situations. The model equations for the single particle model consist of the solid phase diffusion equation (Fick's diffusion law) in a spherical particle and the Butler Volmer equation for each electrode:

$$\frac{\partial c_{s,i}}{\partial t} = \frac{1}{r^2}\frac{\partial}{\partial r}\left(D_{s,i} r^2 \frac{\partial c_{s,i}}{\partial r}\right)$$
$$-D_{s,i}\frac{\partial c_{s,i}}{\partial r}\bigg|_{r=0} = 0 \qquad (1)$$
$$-D_{s,i}\frac{\partial c_{s,i}}{\partial r}\bigg|_{r=R_{s,i}} = \frac{j_{int,i}}{F}$$

$$j_{int,i} = k_i c_e^{0.5}(c_{max} - c_{s,i}|_{r=R_{s,i}})^{0.5} c_{s,i}|_{r=R_{s,i}}^{0.5}$$
$$\left[\exp\left(\frac{0.5F}{RT}(\Phi_i - U_i)\right) - \exp\left(\frac{-0.5F}{RT}(\Phi_i - U_i)\right)\right] \qquad (2)$$

The intercalation current density $j_{int,i}$ is calculated based on the equivalent electro-active surface area (A_i) of the electrode "i":

$$j_{int,i} = \frac{I_{app}}{A_i} = \frac{I_{app}}{((3/R_{s,i})\varepsilon_{s,i} V_i)} \qquad (3)$$

where V_i is the volume of the electrode calculated based on the length, width and thickness of the electrode. It is assumed to be constant during the aging process. $\varepsilon_{s,i}$ is the volume fraction of the active material, which is defined as the ratio between the volume of the active material over the volume of the electrode V_i. The decrease of the volume fraction $\varepsilon_{s,i}$ indicates a loss of active material in the electrode, which could be caused by the isolation of active material particles from the electrode matrix (mechanical failure), etc.

The pseudo steady state method (PSS) [7,8] was used to simplify the diffusion equation from a partial differential equation (PDE) with time and space dependence to a set of differential and algebraic equations (DAEs) with only time dependence. The PSS equations for the diffusion in the solid particles are

$$\frac{\partial \bar{c}_{s,i}}{\partial t} = -\frac{3}{R_{s,i}}\frac{j_{int,i}}{F} \qquad (4)$$

$$(c_{s,i}|_{r=R_{s,i}} - \bar{c}_{s,i}) = -\frac{j_{int,i}}{F}\frac{R_{s,i}}{5D_{s,i}} + \frac{2R_{s,i}}{D_{s,i}}\frac{j_{int,i}}{F}$$
$$\sum_{m=1}^{n}\frac{\sqrt{1+\lambda_m^2}}{\lambda_m^3}(-1)^m \sin(\lambda_m)\, e^{-\lambda_m^2 D_{s,i} t/R_{s,i}^2} \qquad (5)$$

where the number of terms "n" in the summation is typically set equal to 5; $\bar{c}_{s,i}$ is the volume averaged concentration in the spherical particle and $c_{s,i}|_{r=R_{s,i}}$ is the concentration at the surface of the particle. The state of charge or the stoichiometric number of the electrode is defined as

$$x_i = \frac{\bar{c}_{s,i}}{c_{max,i}} \qquad (6)$$

The λ_m values are determined from the eigen-value equation:

$$\lambda_m = \tan(\lambda_m) \qquad (7)$$

The single particle model is used to fit the low rate (C/33) experimental data from the rate capability tests. Four model parameters are found to change with storage time when fitting the C/33 rate discharge curves. The model parameters are initial state of charge (x_0) of the anode and the cathode at the beginning of discharge and the volume fraction (ε_s) of the active materials in both electrodes. The least square regression method [9] was used to fit the experimental data with the single particle model. It was assumed that the kinetic and transport limitations are not important during the low rate discharge in the fitting process.

4. Results and discussion

Fig. 3 compares the C/33 discharge profiles for fresh cells stored at different temperatures. The parameter values are compared in Fig. 4. The values of the volume fractions (ε_s) are close, indicating that the fresh cells have similar amounts of active materials in the electrodes. The SOC of the $LiCoO_2$ electrode

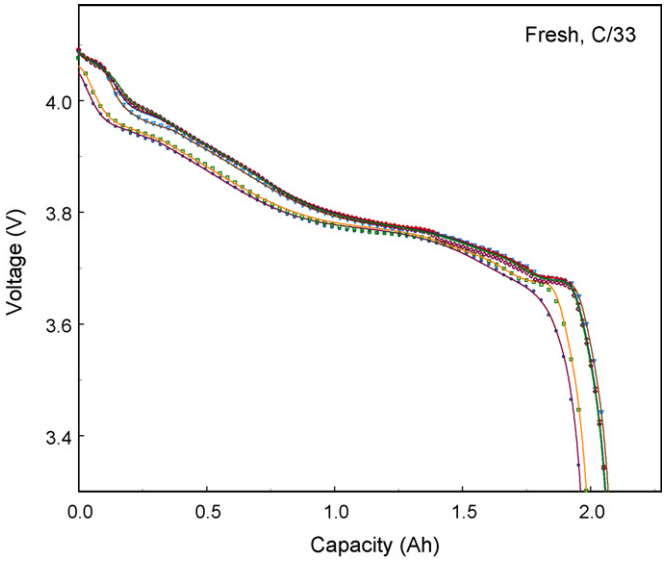

Fig. 3. Discharge profiles for fresh cells stored at different temperatures (C = 1.656 A). The profiles from the top to the bottom are 45–5 °C. The points are experiment data and the lines are the simulated profiles.

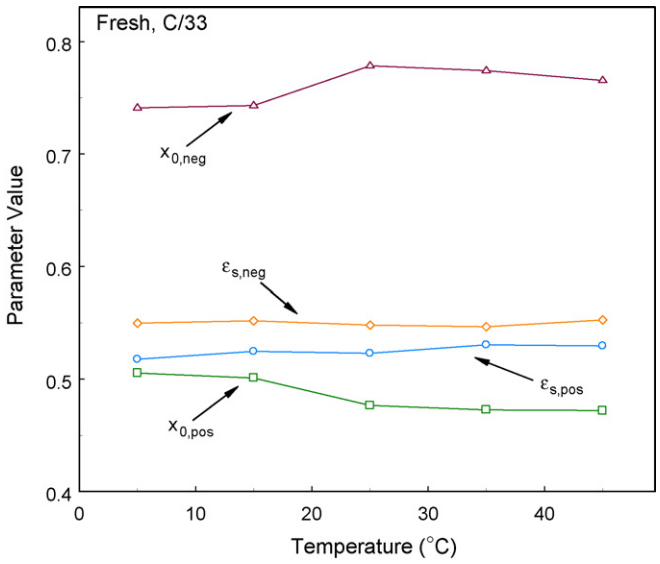

Fig. 4. The fitting parameter values for fresh cells at different temperatures. Both the $LiCoO_2$ and carbon electrodes become less charged (i.e., larger $x_{0,pos}$ and smaller $x_{0,neg}$) at low temperatures.

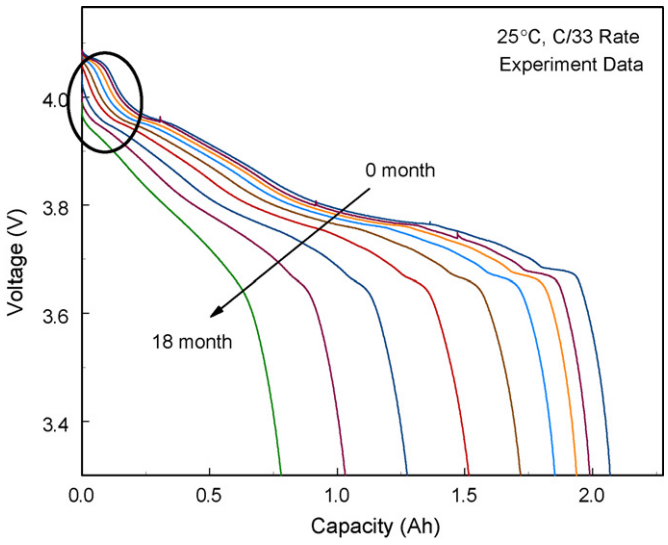

Fig. 6. The experimental discharge profiles taken in the rate capability tests at 25 °C. The fact that less ripples are observed at the beginning of discharge profiles indicates that the $LiCoO_2$ electrode is gradually less charged.

($x_{0,pos}$) at the beginning of discharge decreases as the temperature increases. The cathode becomes more charged at higher temperatures. This is directly reflected in the experimental profiles as there are fewer ripples on the top of the discharge profiles at low temperatures, as shown in Fig. 3. The ripples are characteristic of the open circuit potential (OCP) of the $LiCoO_2$ electrode, as shown in Fig. 5. The presence of these characteristic ripples makes it relatively easy to locate $x_{0,pos}$ for the $LiCoO_2$ electrode. By carefully observing the ripples on the low rate profiles, one can tell whether the $LiCoO_2$ electrode is charged to a higher or lower stoichiometric number (or SOC). For example, Fig. 6 shows the C/33 rate discharge profiles measured at 25 °C in the rate capability tests. The experimental data show that there are fewer ripples at the beginning of the discharge profiles after storage. This indicates that the aged $LiCoO_2$ electrodes become increasingly less charged after storage, even though the end of charge voltage (EOCV) for the full cell remained the same. The simulation also shows that the carbon electrode becomes less charged at low temperatures (with smaller $x_{0,neg}$), which causes the cells to deliver less capacity.

Figs. 7 and 8 present comparison of the experimental and simulated discharge profiles at C/33 rate for 5 and 15 °C, respectively. The changes of the four fitting parameters with storage time are displayed in Figs. 9 and 10, respectively. The capacity fade and the change of fitting parameters at 5 and 15 °C follows similar pattern. The aged $LiCoO_2$ cathode becomes increasingly less charged, as the stoichiometric number ($x_{0,pos}$) of the cathode increases slightly with time. The anode also becomes less charged (with smaller $x_{0,neg}$). The volume fraction of active

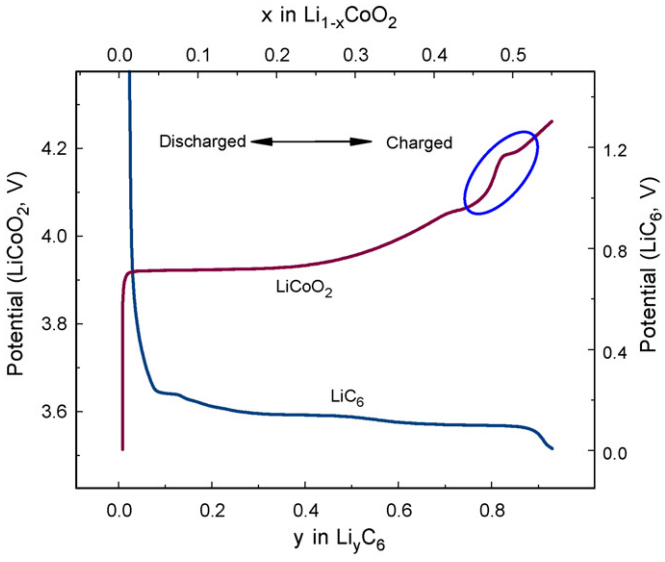

Fig. 5. The open circuit potentials for the $LiCoO_2$ and carbon electrode.

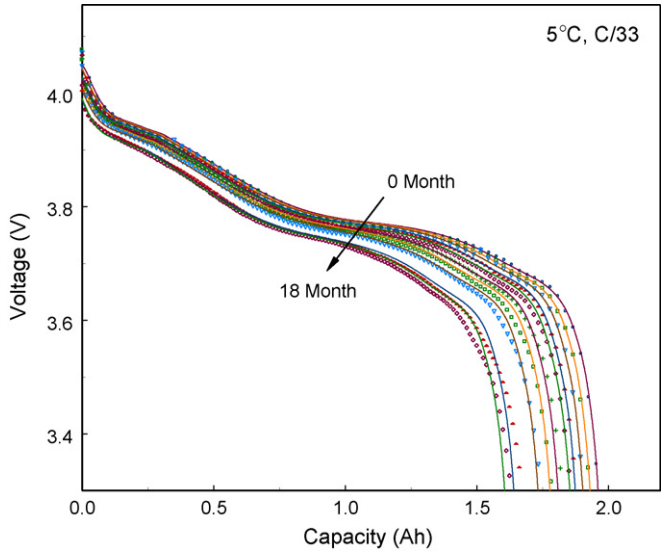

Fig. 7. Comparison of experiment and simulated discharge profiles at 5 °C.

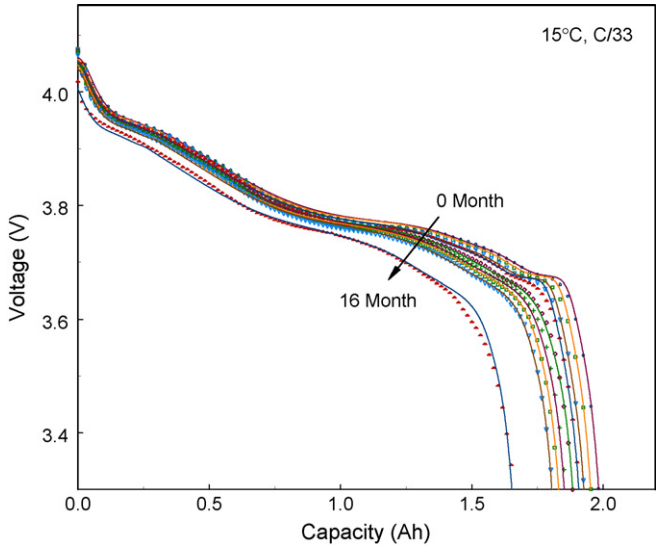

Fig. 8. Comparison of experiment and simulated discharge profiles at 15 °C.

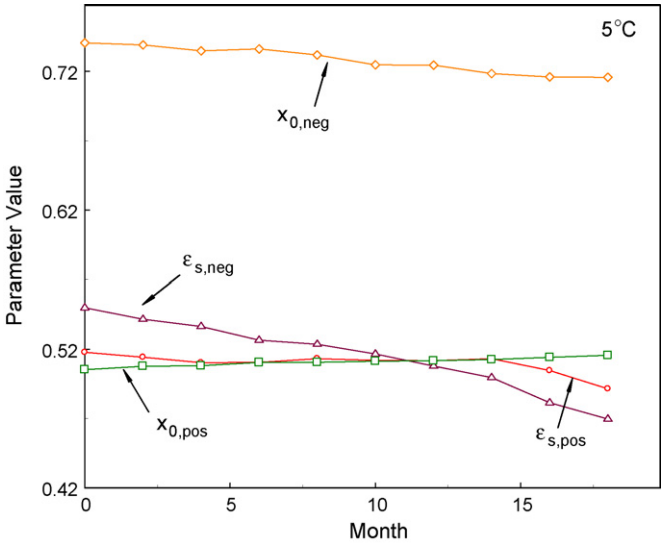

Fig. 9. Change of fitting parameter values with storage time at 5 °C.

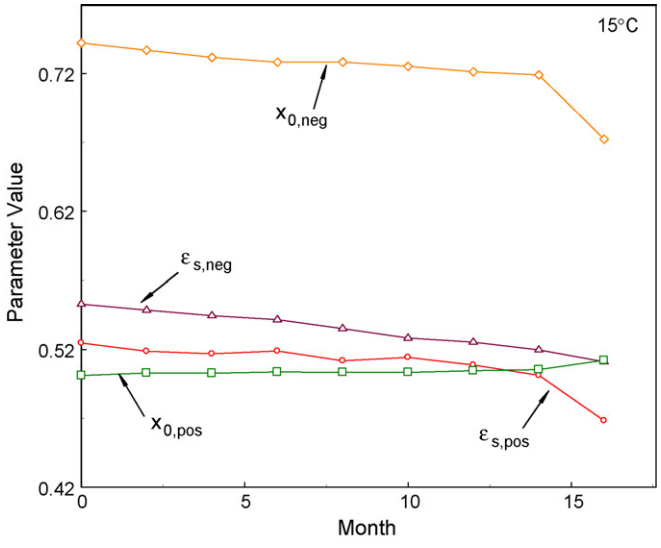

Fig. 10. Change of fitting parameter values with storage time at 15 °C.

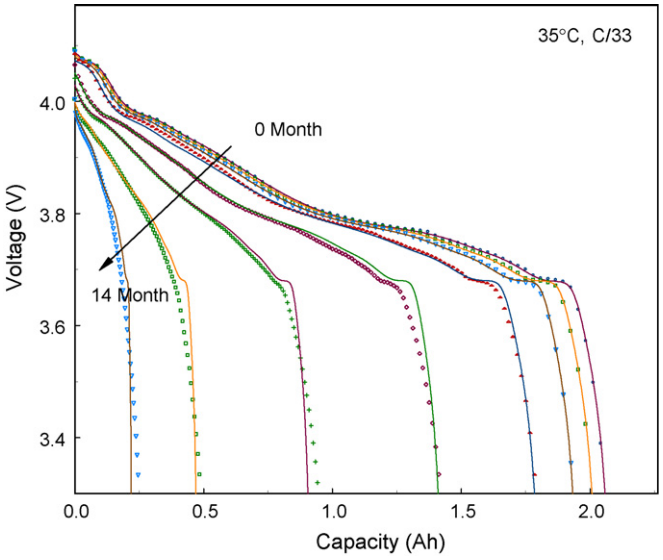

Fig. 11. Comparison of experiment and simulated discharge profiles at 35 °C.

material in the anode $\varepsilon_{s,neg}$ decreases after storage at float charge condition. This indicates that some electro-active surface area becomes inaccessible after storage because of the deposition of side reaction products and/or some carbon particles become mechanically isolated from the electrode and inactive for the insertion reaction. The parameter $\varepsilon_{s,pos}$ does not change much with storage at these temperatures. The model parameters are shown to change largely in a linear pattern, consistent with the linear capacity fade of the full cells.

Figs. 11 and 12 compare the experimental and simulated discharge profiles at 35 and 45 °C. The changes of fitting parameter values with storage time are shown in Figs. 13 and 14. The volume fractions drop slightly in the first few months of storage where the capacity fade is small. Then the volume fraction drops at a much faster pace and the capacity fade of the cells also accelerates. The decrease of the volume fractions of active

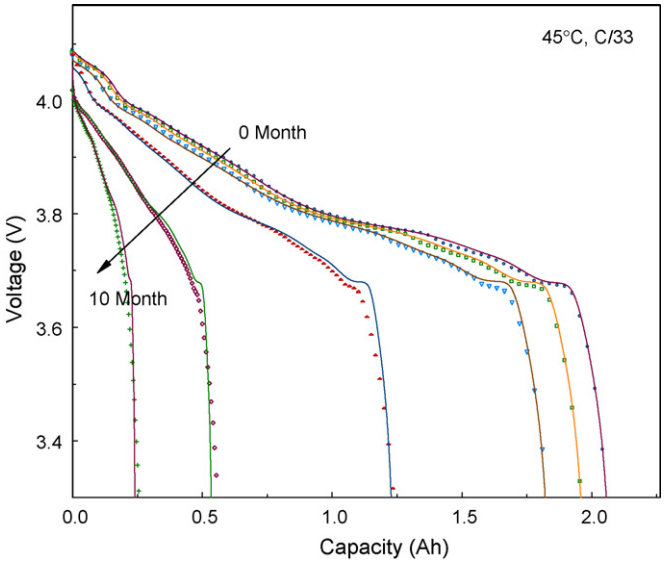

Fig. 12. Comparison of experiment and simulated discharge profiles at 45 °C.

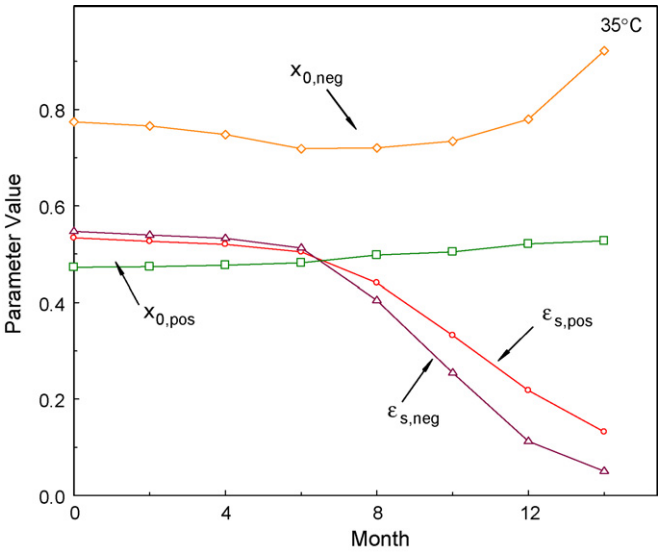

Fig. 13. Change of fitting parameter values with storage time at 35 °C.

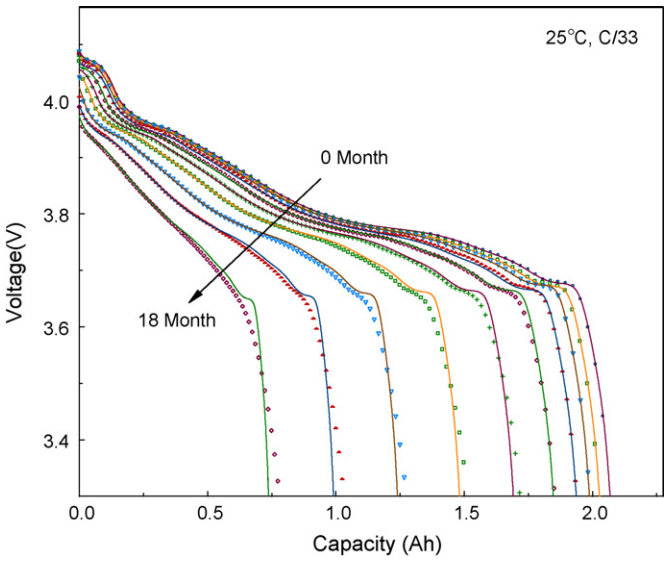

Fig. 15. Comparison of experiment and simulated discharge profiles at 25 °C.

materials is much more significant at high temperatures than that at low temperatures. These results suggest that there could be two different mechanisms controlling the capacity fade at these temperatures. The capacity fade was initially caused mostly by the loss of lithium ions due to side reactions. Then the capacity fade becomes controlled by the rapid loss of active material in the electrodes. Our half-cell study [4] showed that there were significant losses of active material in the used electrodes taken from the aged cells. We think the loss is mostly caused by the mechanical changes of the electrodes, where the solid particles gradually lose contact with the electrode during storage (at float charge condition). The stoichiometric number for the anode in the charged state ($x_{0,neg}$) decreases when the capacity fade is mostly caused by the loss of lithium inventory. However, when the capacity fade is controlled by the loss of active materials, the $x_{0,neg}$ starts to increase, indicating that the anode is charged to a higher SOC. A plausible explanation for the behavior of $x_{0,neg}$ is that the active material loss in the anode is so severe that it outpaces the loss of lithium inventory in the system. Thus, the remaining active carbon material in the anode needs to be charged to a higher SOC to accommodate the lithium ions transferred from the cathode. The stoichiometric number of the cathode gradually increases during capacity fade, meaning the cathode becomes less charged. This result is consistent with the experimental observation; that is, the characteristic ripples from the cathode gradually disappear in the discharge profiles as storage time increases.

Comparisons of the experimental and simulated profiles at 25 °C are presented in Fig. 15. The changes of fitting parameters with storage time are shown in Fig. 16. The model parameters change in similar patterns as those at higher temperatures, except the stoichiometric number of the anode ($x_{0,neg}$). The $x_{0,neg}$

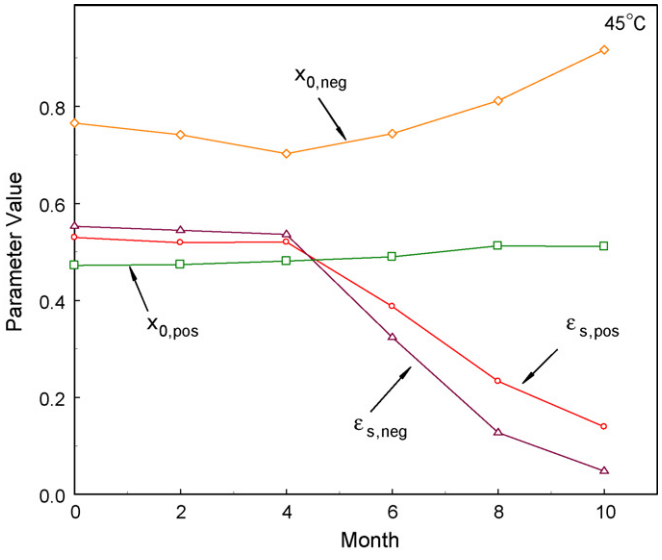

Fig. 14. Change of fitting parameter values with storage time at 45 °C.

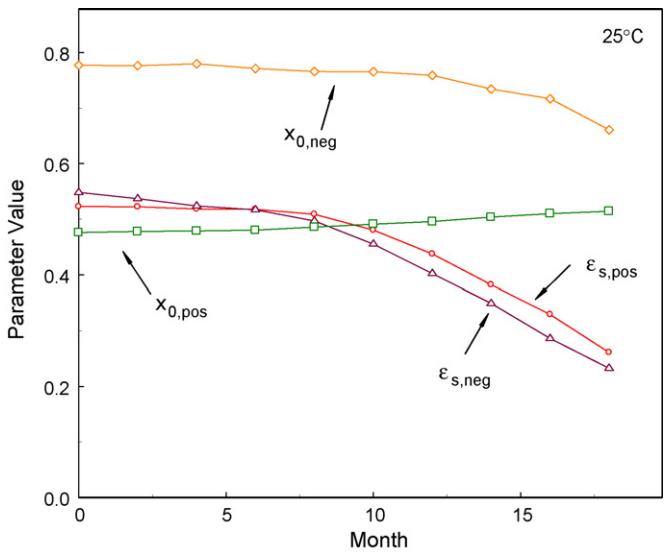

Fig. 16. Change of fitting parameter values with storage time at 25 °C.

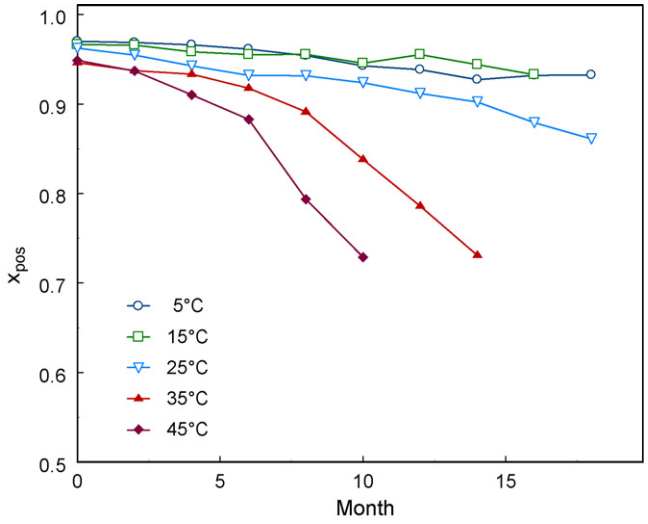

Fig. 17. The simulated x_{pos} (SOC at the end of low rate discharge) for the $LiCoO_2$ electrodes after storage.

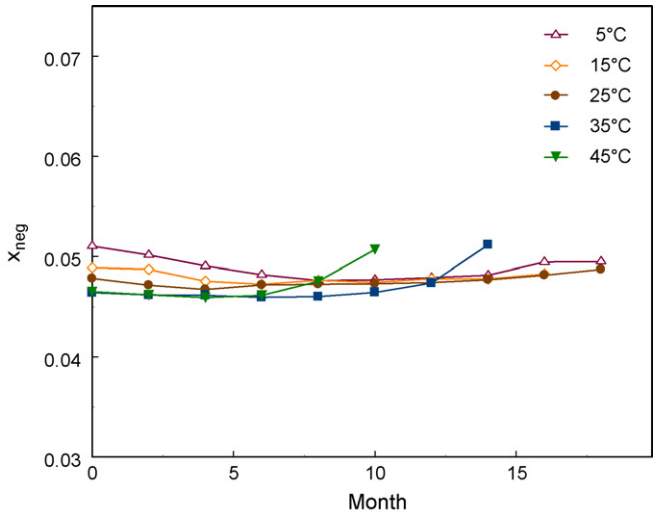

Fig. 18. The simulated x_{neg} (SOC at the end of low rate discharge) for the carbon electrodes after storage.

decreases continuously with capacity fade at 25 °C. An explanation for this could be that the loss of active carbon material at 25 °C is not severe enough to outpace the loss of lithium inventory. Thus loss of active material in the anode could not trigger the change of the parameter $x_{0,neg}$ at 25 °C as it does at higher temperatures.

With the model parameters readily available for each discharge curve, it is of interest to see what the stoichiometric numbers (SOC) would be at the end of the low rate discharge for the cathode and the anode.

Fig. 17 shows the simulated stoichiometric numbers for the cathodes stored at different temperatures. When cyclable lithium ions are irreversibly lost in the charge/discharge process, there are not enough of them available in the cell to intercalate the cathode fully back to the fresh state. The consequence of this is that the cathode is gradually emptied, as confirmed by the increasingly smaller stoichiometric numbers. The smaller the stoichiometric number (x_{pos} in the figure), the less the $LiCoO_2$ electrode is intercalated. Fig. 17 also shows the temperature effect on the x_{pos}. As the cells lose capacity (lithium inventory) faster and greater at increased temperatures, the stoichiometric numbers also decrease faster and steeper. Fig. 18 shows the stoichiometric numbers for the carbon electrode (x_{neg}) at the end of discharge after storage. The carbon electrode appears to be mostly discharged to the same x_{neg} all the time except at high temperatures, where the anode becomes slightly less discharged.

Based on our simulations, it is clearly shown that the stoichiometric window of the $LiCoO_2$ electrode shrinks with capacity fade after cells are stored for some time under float charge conditions. That is, the fresh $LiCoO_2$ electrode might be cycled between the × marker (at charged state) and the ◯ marker (at discharged state) as shown in Fig. 19 when the cell is cycled between 3.3 and 4.1 V. After storage, the aged $LiCoO_2$ electrode could not be charged to the same stoichiometric number (× marker) even though the charge protocol remains the same, because of the increased cell impedance. The aged $LiCoO_2$ electrode could not be discharged to the same SOC (◯ marker) with the same discharge protocol because of the loss of lithium inventory. Consequently, the stoichiometric window on the $LiCoO_2$ electrode shrinks with capacity fade in this calendar life study. The simulation also shows that the downward movement of the × marker is relatively small, but the upward movement of the ◯ marker is more obvious and is closely related to the degree of cell capacity fade.

The change of the stoichiometric window on the carbon electrode is more complicated. The fresh carbon electrode might be cycled between the × marker (at charged state) and the ◯ marker (at discharged state) as shown in Fig. 20. The movement of the × marker for an aged carbon electrode depends on the controlling capacity fade mechanisms (loss of Li^+ ions or loss of active carbon). At low temperatures, the capacity fade is mostly caused by loss of cyclable lithium ions. The carbon electrode gradually becomes less charged, that is, the × marker moves to the left in Fig. 20. At high temperatures (in Figs. 13 and 14), when the

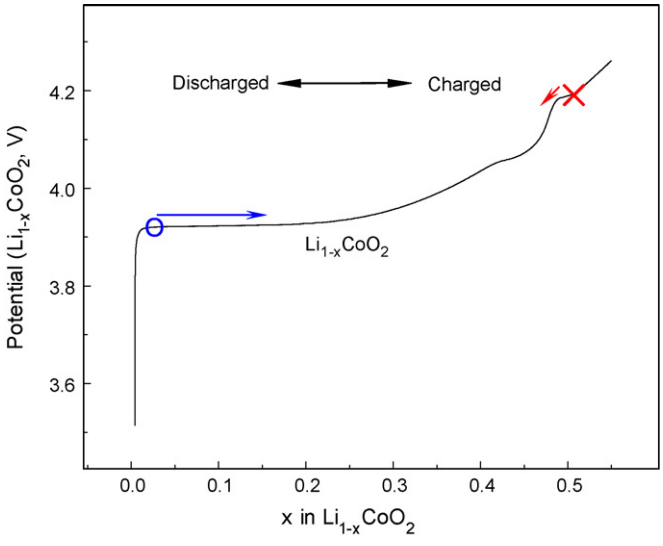

Fig. 19. The shrinkage of the stoichiometric window for the cathode with capacity fade.

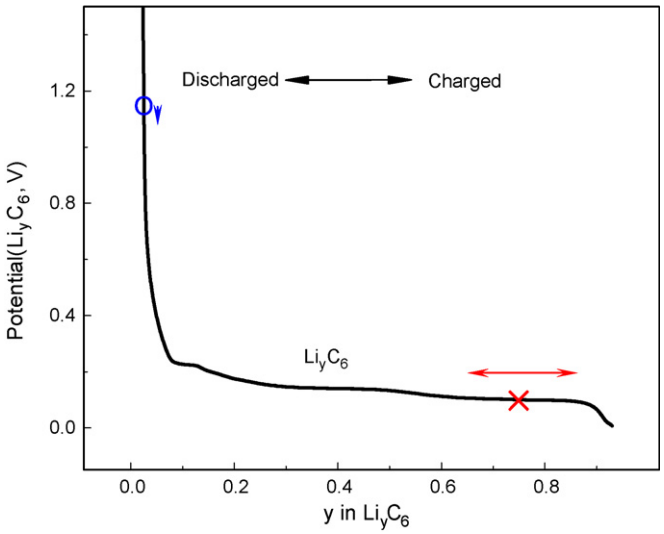

Fig. 20. The change of the stoichiometric window for the anode after storage (at float charge condition). The anode becomes less charged when the capacity fade is caused mostly by the loss of cyclable lithium ions. The anode would be charged to a higher SOC when the loss of active materials controls the capacity fade and outpace the loss of lithium ions.

capacity fade is initially controlled by the loss of cyclable lithium ions, the × marker moves to the left (the anode is less charged). When the loss of active materials becomes severe enough to outpace the loss of lithium inventory and controls the capacity fade, the anode turns to be charged to a higher SOC and the × marker moves to the fight in Fig. 20. The aged carbon electrodes appear to be discharged mostly to the same SOC (the ◯ marker). At high temperatures, the anode tends to become slightly less discharged and the ◯ marker moves a little bit downward in Fig. 20.

5. Conclusions

Our experiment results showed that the loss of active materials in the electrodes and the loss of cyclable lithium ions were the major capacity fade mechanisms responsible for the cell capacity fade at low C/33 rate in a calendar life study. But the experiment provided little information on how the two mechanisms evolve with cell capacity fade. In this work, we analyzed the experimental data numerically with a single particle model. Our simulation results suggest that the cell capacity fade could have different controlling mechanisms at different temperatures. The capacity fade at low temperature is mostly caused by the loss of the lithium ion inventory, with only minor loss of active materials in the electrodes. At high temperatures, the cell capacity fade exhibits a two regime pattern, where the loss of lithium ion inventory and the severe loss of active materials controls the capacity fade at the respective regime.

In addition, we also investigated the changes of the stoichiometric windows for the cathode and the anode with cell capacity fade. The stoichiometric window for the $LiCoO_2$ electrode shrinks with cell capacity fade. The change of the stoichiometric window on the anode is more complicated and depends on the controlling capacity fade mechanisms. When the capacity fade is caused mostly by Li^+ loss, the anode becomes consistently less charged. When the loss of active material in the anode controls the capacity fade and outpaces the loss of lithium ion inventory, the anode is gradually charged to a higher SOC, in danger of becoming overcharged at high temperatures such as 35 and 45 °C.

Acknowledgement

The authors are grateful for the financial support of the project by the National Reconnaissance Office (NRO) under contract #NRO-000-03-C-0122.

References

[1] B.Y. Liaw, R.G. Jungst, G. Nagasubramanian, H.L. Case, D.H. Doughty, J. Power Sources 140 (2005) 157.
[2] A.T. Stamps, C.E. Holland, R.E. White, E.P. Gatzke, J. Power Sources 150 (2005) 229.
[3] P. Ramadass, B. Haran, R.E. White, B.N. Popov, J. Power Sources 123 (2003) 230.
[4] Q. Zhang, R.E. White, J. Power Sources 173 (2007) 990.
[5] G. Ning, B.N. Popov, J. Electrochem. Soc. 151 (2004) A1584.
[6] S. Santhanagopalan, Q. Guo, P. Ramadass, R.E. White, J. Power Sources 156 (2006) 620.
[7] Q. Zhang, R.E. White, J. Power Sources 165 (2007) 880.
[8] S. Liu, Solid State Ionics 177 (2006) 53.
[9] A. Constantinides, N. Mostoufi, Numerical Methods for Chemical Engineers with MATLAB Applications, Prentice Hall, PTR, 1999.